NANO LETTERS

pubs.acs.org/NanoLett Letter

Matairesinol Nanoparticles Restore Chemosensitivity and Suppress Colorectal Cancer Progression in Preclinical Models: Role of Lipid Metabolism Reprogramming

Shenshen Wu, Jiajia Wang, Zan Fu, Giuseppe Familiari, Michela Relucenti, Michael Aschner, Xiaobo Li, Hanqing Chen,* and Rui Chen*

Cite This: https://doi.org/10.1021/acs.nanolett.3c00035 Read Online

ABSTRACT: Oncogenic-driven lipogenic metabolism is a common hallmark of colorectal cancer (CRC) progression. Therefore, there is an urgent need to develop novel therapeutic strategies for metabolic reprogramming. Herein, the metabolic profiles in the plasma between CRC patients and paired healthy controls were compared using metabolomics assays. Matairesinol downregulation was evident in CRC patients, and matairesinol supplementation significantly represses CRC tumorigenesis in azoxymethane/dextran sulfate sodium (AOM/DSS) colitis-associated CRC mice. Matairesinol rewired lipid metabolism to improve the therapeutic efficacy in CRC by inducing mitochondrial damage and oxidative damage and blunting ATP production. Finally, matairesinol-loaded liposomes significantly promoted the enhanced antitumor activity of 5-Fu/leucovorin combined with oxaliplatin (FOLFOX) in CDX and PDX mouse models by restoring chemosensitivity to the FOLFOX regimen. Collectively our findings highlight matairesinol-mediated lipid metabolism reprogramming as a novel druggable strategy to restore CRC chemosensitivity, and this nanoenabled approach for matairesinol will improve the chemotherapeutic efficacy with good biosafety.

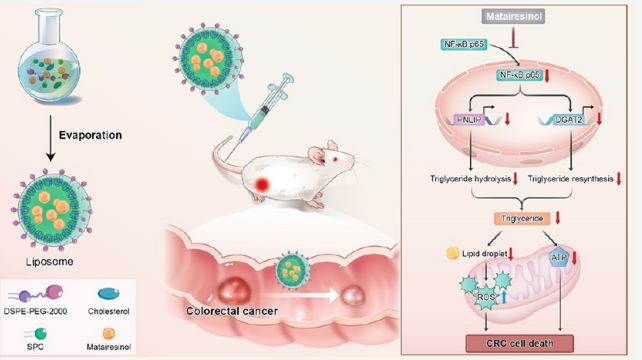

KEYWORDS: *colorectal cancer, liposome nanoparticles, metabolomics, triglyceride metabolism, lipid droplet*

Colorectal cancer (CRC) is one of the most commonly diagnosed malignancies worldwide and results in an estimated 900 000 deaths annually.[1] Although better screening and advances in surgical treatment have been achieved for CRC therapy, the long-term outcome of CRC patients remains not optimistic, and over 90% of metastatic CRC patients encounter treatment failure due to chemotherapy resistance.[2] Thus, identifying a potential predictor and revealing the underpinning mechanism are urgently warranted for preventing CRC development and recovering chemosensitivity.

Metabolomics focuses on measuring the individual alterations of low-molecular-weight metabolites in response to a pathophysiological stimulus or genetic modification.[3,4] As metabolites comprise the end products of gene expression and enzyme activities of organisms, the investigation of metabolites can help understand the consequences of the altered gene and protein expression, enzyme activities, and signaling pathways.[4] Therefore, the characterization of metabolite signatures has been extensively incorporated into disease diagnosis, outcome prediction, customized drug treatments, and development of novel therapeutic approaches.[5−10] Several studies on metabolic profiling have been performed to identify key metabolic compounds involved in CRC development,[11] monitor CRC progression,[12] and predict the survival of patients with CRC.[13] Using mass spectrometry (MS)-based serum metabolic profiling, Leichtle et al. identified serum glycine and tyrosine in combination with carcinoembryonic antigen (CEA) as being superior to CEA alone in the detection of CRC in patients.[14] Răchieriu et. al confirmed the association between upregulated lipogenesis and CRC progression using UPLC-QTOF-ESI$^+$MS.[15] Nevertheless, few metabolites have been translated into clinical applications.

To develop a metabolite-based therapeutic strategy for CRC treatment, we performed an unbiased GC-MS-based metabolomics of blood plasma from 100 CRC patients and paired healthy controls. The demographic and clinical information on subjects are summarized in Table S1. A total of 46 differential

Received: January 4, 2023
Revised: February 12, 2023

https://doi.org/10.1021/acs.nanolett.3c00035
Nano Lett. XXXX, XXX, XXX−XXX

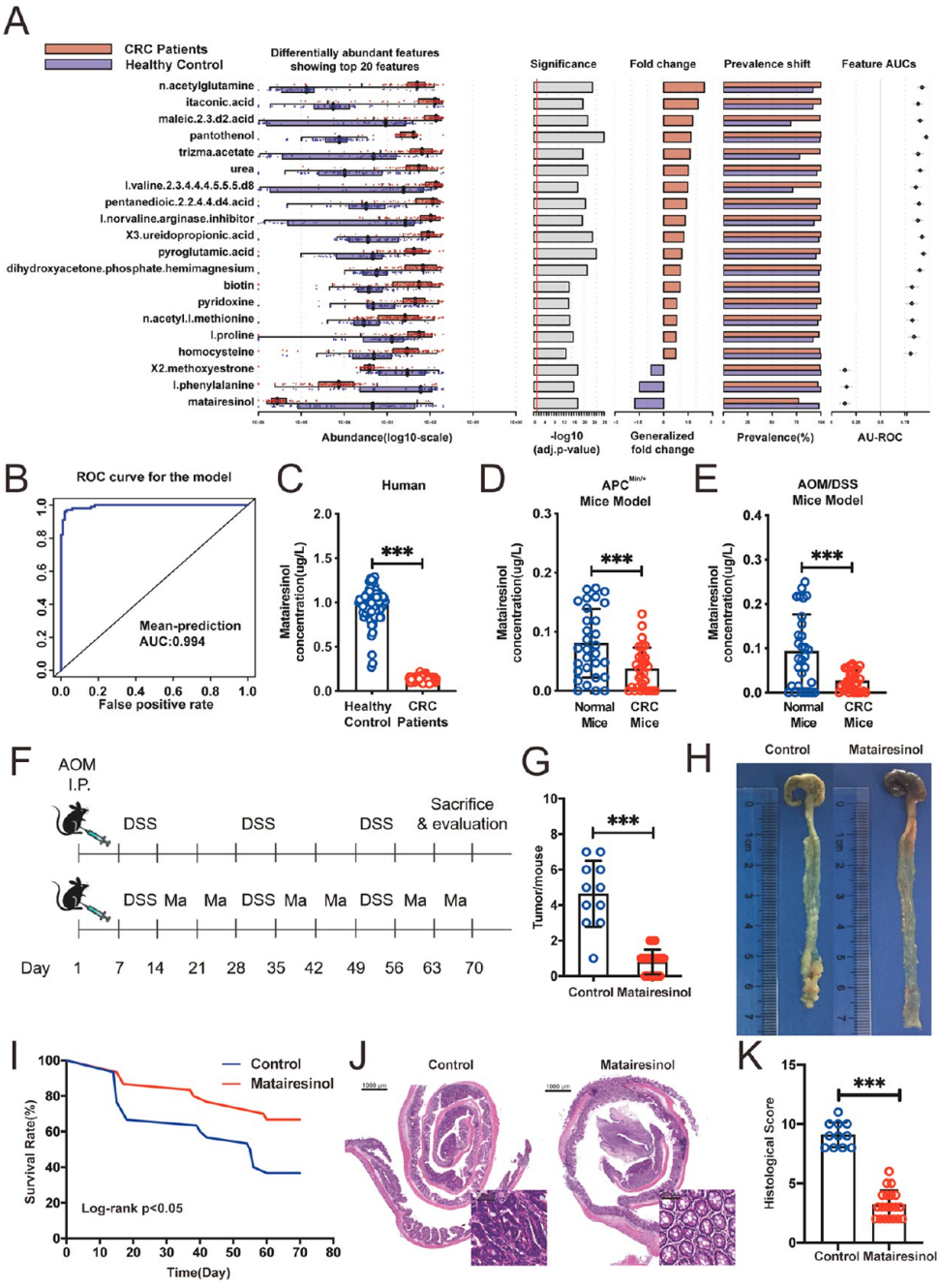

Figure 1. Metabolic marker matairesinol is diminished in CRC and protects against tumor development. (A) The top 20 differential modulated metabolites in CRC patients, relative to healthy controls. (B) ROC curves derived from lasso regression for segregating healthy subjects from CRC patients. (C) Quantification of matairesinol in plasma samples of patients with CRC and healthy controls in the testing cohort (n = 100 each, ***P < 0.001, compared with healthy controls, two-tailed t-test, error bars, S.D.). (D, E) Quantification of plasma matairesinol in (D) $APC^{Min/+}$ and (E) colitis-associated CRC murine models. (n = 30 each, ***P < 0.001, compared with the mice-with-tumor group, two-tailed t-test, error bars, S.D.). (F) Schematic of the generation of the colitis-associated CRC model (n = 30/group). (G) Macroscopic tumor numbers and (H) colon length of mice (n = 11 in the control group and n = 20 in the matairesinol-treated group, ***P < 0.001, compared with the control group, two-tailed t-test, error bars, S.D.). (I) Overall survival of mice assessed using the Kaplan−Meier method (Log-rank p < 0.05). (J) Representative images and (K) colitis scores of H&E staining on distal colonic sections (n = 11 in the control group and n = 20 in the matairesinol-treated group, ***P < 0.001, compared with the control group, two-tailed t-test, error bars, S.D.).

metabolites were identified, and the top 20 differentially metabolites are shown in Figure 1A. To confirm the above results and better distinguish the metabolite most significantly induced during CRC initiation, we further performed a CRC prediction model using lasso regression. Among them, 15 metabolites were identified as the potential distinguished predictors for CRC progression (Figure S1A). The value for the area under the ROC curve (AUC) was 99.4% (Figure 1B). We next performed the targeted UPLC-MS/MS method to identify the top three discriminated metabolites (matairesinol, l.phenylalanine, and X2.methoxyestrone) and found only matairesinol was decreased in the CRC group (Figure 1C). The mean concentrations of matairesinol in healthy controls and CRC patients were 0.9720 ± 0.0243 and 0.1419 ± 0.1745

https://doi.org/10.1021/acs.nanolett.3c00035
Nano Lett. XXXX, XXX, XXX−XXX

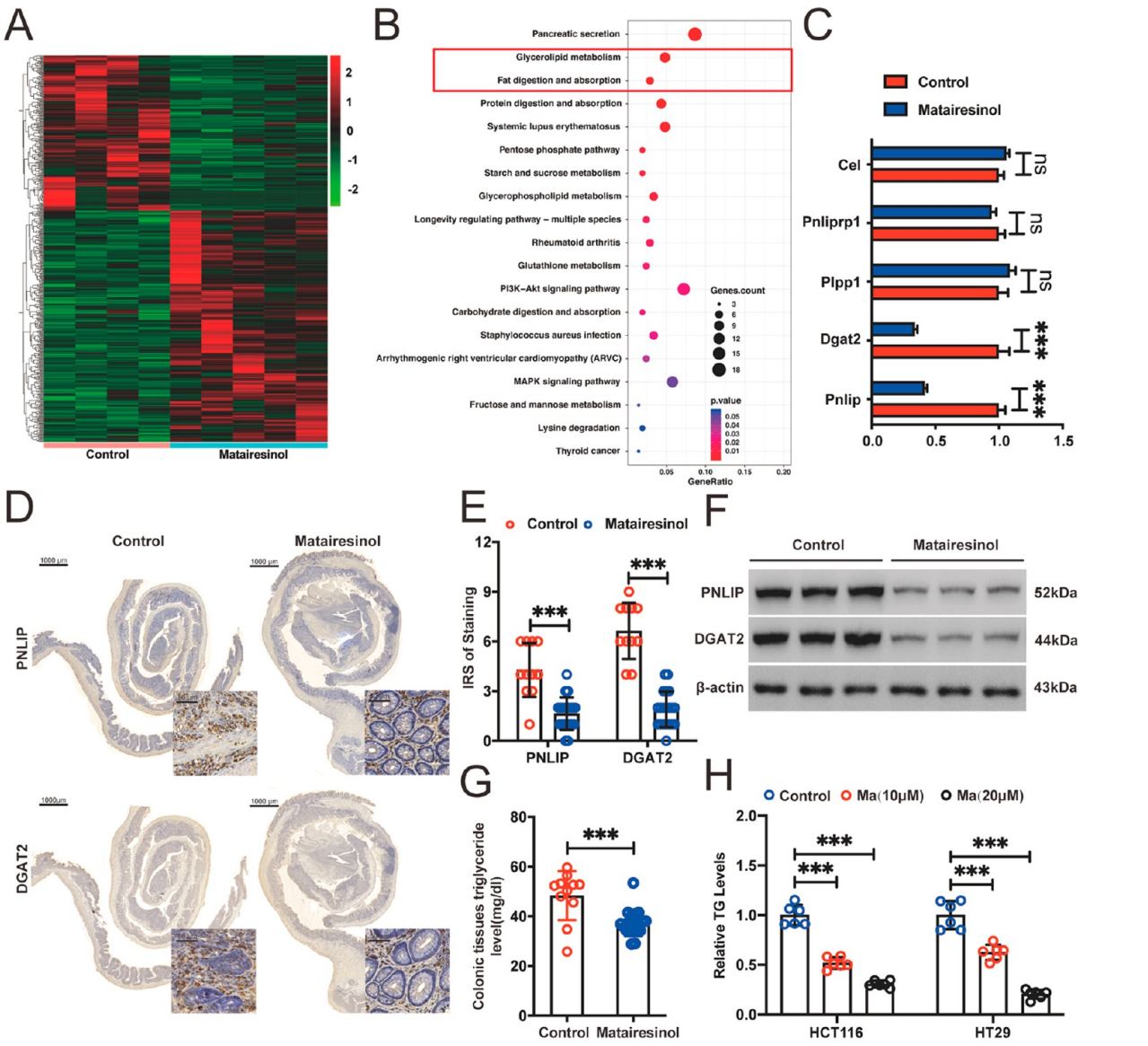

Figure 2. Matairesinol decreases triglyceride by regulating PNLIP and DGAT2 expression. (A) Heatmap of gene expression in control or matairesinol-treated murine colons. The down-regulation and up-regulation of genes are expressed by green and red color, respectively. (B) Enriched KEGG pathways of the differentially expressed genes identified in the RNA-Seq assay. (C) Heat-map of fat digestion and absorption and glycerolipid metabolism pathway-involved mRNA (n = 11 in the control group and 20 in the matairesinol-treated group). The downregulation and up-regulation of genes are expressed by green and red color, respectively. (D) Representative images and (E) immunoreactive score (IRS) of PNLIP and DGAT2 in colonic tissues of mice, as determined by IHC (n = 11 in the control group and n = 20 in the matairesinol-treated group, ***P < 0.001, compared with the control group, two-tailed t-test, error bars, S.D.). (F) PNLIP and DGAT2 protein levels in the colonic tissues of mice were determined by WB (n = 3 in each group). (G) Quantification of colonic triglycerides (TGs) in the colitis-associated cancer model (n = 11 in the control group and n = 20 in the matairesinol-treated group, ***P < 0.001, compared with the control group, two-tailed t-test, error bars, S.D.). (H). Effect of matairesinol on TGs levels in colorectal cancer cells. ***P < 0.001, calculated using one-way ANOVA.

μg/L, respectively (Figure 1C). Similarly, decreased matairesinol was further confirmed in another independent study from 300 pairs of plasma from CRC patients and healthy controls (Figure S1B–E). Moreover, matairesinol was also significantly decreased in tumor-bearing $APC^{Min/+}$ mice or murine AOM/DSS models compared to the tumor-free mice (Figure 1D, E). Collectively, our results indicate that matairesinol is downregulated in the plasma of CRC patients.

To evaluate the potential protective function of matairesinol in CRC therapy, we first compared the cellular effects of matairesinol on normal colonic epithelial NCM460 cells and two human CRC cell lines. Matairesinol treatment significantly inhibited the viability of HT29 and HCT116 cells in a concentration-dependent manner and exerted good biocompatibility and no cytotoxicity on NCM460 cells (Figure S2A). Next, a dose of 10 μM, which would actually correspond to human equivalent intakes of 0.098 mg of matairesinol per day for a 70 kg adult,[16] was chosen for further study. We next investigated whether intragastric administration of matairesinol could inhibit CRC tumorigenesis using a colitis-associated cancer model (Figure 1F). Mice treated with matairesinol showed a significant reduction in tumor numbers (Figure 1G) and increased colon length (Figure 1H and Figure S2B), body weight (Figure S2C), and survival time (Figure 1I). Representative H&E staining images showed that mice treated with matairesinol had higher-grade dysplasia and a lower

https://doi.org/10.1021/acs.nanolett.3c00035
Nano Lett. XXXX, XXX, XXX−XXX

histological score of the tumor compared with control mice (Figure 1J, K). Altogether, these data demonstrate that matairesinol might be pivotal for preventing colitis-associated CRC development in mice.

To elucidate the potential regulatory mechanism of matairesinol in CRC therapy, an RNA-Seq assay was carried out in colonic tissues from AOM/DSS model mice with or without matairesinol treatment. A total of 197 up-regulated and 294 down-regulated mRNAs were identified in matairesinol-treated mice with a cutoff of fold change (FC) > 1.5 and p-value <0.05 (Figure 2A). These differentially regulated genes were then annotated using the Kyoto Encyclopedia of Genes and Genomes (KEGG) pathway database and grouped into glycerolipid metabolism, fat digestion, and absorption pathways (Figure 2B), alterations in which are the key hallmarks in CRC development.[17,18] To gain insights into matairesinol attenuation of the AOM/DSS-induced aberrant metabolism, we investigated the expression of five differentially related genes for colonic lipid metabolism including *Pnlip*, *Dgat2*, *Plpp1*, *Pnliprp1*, and *Cel*. The gene expression of AOM/DSS-induced up-regulation of *Pnlip* and *Dgat2* was significantly decreased by matairesinol administration, and the mRNA levels of expression of *Plpp1*, *Pnliprp1*, and *Cel* were comparable between both groups of mice (Figure 2C). Similarly, matairesinol treatment induced 61% and 71% reduction of the levels of PNLIP and DGAT2 proteins in the colon of CRC mice, respectively (Figure 2D−F). Moreover, matairesinol administration significantly suppressed the expression of *PNLIP* and *DGAT2* in HCT116 and HT29 cells in a concentration-dependent manner (Figure S3A, B). Both of PNLIP and DGAT2 protein expression were negatively correlated to plasma matairesinol levels in AOM/DSS model mice (Figure S3C, D). Taken together, matairesinol inhibits the AOM/DSS-induced activation of PNLIP and DGAT2, which may prevent the development of CRC.

TGs are the major storage molecules of metabolic energy and fatty acids,[19] originating from either dietary or endogenous sources. Dietary TGs are hydrolyzed to monoacylglycerols and free fatty acids by PNLIP in the intestinal lumen following ingestion, which are subsequently absorbed by enterocytes and re-esterified to diacylglycerol in a reaction catalyzed by monoacylglycerol acyltransferase. DGAT then facilitates triacylglycerol resynthesis from monoacylglycerol,[20] which was considered the final and committed step for triglyceride synthesis. Thus, DGAT2 and PNLIP are the key enzymes in the regulation of triglyceride (TG) hydrolysis and resynthesis, which is associated with TG homeostasis;[21] we further investigated the regulatory role of matairesinol in TG accumulation in CRC development. Matairesinol treatment significantly decreased colonic TG accumulation in AOM/DSS-treated mice (Figure 2G) and reduced the TG levels in HCT116 and HT29 cells compared to the controls (Figure 2H). Moreover, colonic TG levels were positively correlated with the protein levels of PNLIP and DGAT2 in the colon of AOM/DSS-treated mice (Figure S3E, F). Based on the aforementioned results, we may infer that matairesinol treatment attenuates colonic TG accumulation and represses CRC tumorigenesis by downregulating PNLIP and DGAT2.

Previous studies have shown that matairesinol is a potent inhibitor of the IKK-β enzyme with favorable binding affinity[22] and decreased phosphorylation level of NF-kB/p65,[23] which is a promising resource for cancer drug discovery. By using the AliBaba2.1 software,[24] we found that NF-kB p65 harbors a binding site to both PNLIP and DGAT2 promoter regions. We hypothesized that matairesinol regulates the expression of PNLIP and DGAT2 in CRC development by blunting the activity of the IKK-β enzyme and NF-kB p65 signaling. Matairesinol treatment significantly reduced the phosphorylation of IκBα and p65 and inhibited the degradation of IκBα in HCT116 and HT29 cells (Figure S4A), which indicated the reduced translocation of NF-κB/p65 into the nucleus and the initiation of transcription. As expected, a blunted nuclear translocation of NF-κB/p65 was found in HCT116 and HT29 cells after being treated with matairesinol (Figure S4B). Inhibition of the binding affinity of NF-κB p65 to PNLIP and DGAT2 promoter region was evidenced in both CRC cells with matairesinol treatment (Figure S4C, D). Similarly, matairesinol-treated CRC cells showed a significant inhibition on NF-κB luciferase activity (Figure S4E). Moreover, matairesinol treatment led to decreased levels of PNLIP and DGAT2 protein, and such inhibition was rescued by NF-κB p65 overexpression (Figure S4F). These findings suggested that matairesinol attenuated the altered lipid metabolism and decreased TG accumulation in CRC through inhibiting NF-κB/p65 mediated transcriptional regulation on PNLIP and DGAT2.

Increased lipid droplet (LD) accumulation has been identified as a prominent characteristic of cancer.[25] LDs, as specific lipid-storage organelles, are formed *de novo* following the synthesis of TGs.[26,27] The hydrophobic core of LD is formed by the TG pathway called the glycerol-phosphate pathway, which was terminated by both diacylglycerol O-acyltransferase enzymes DGAT1 and DGAT2.[28] LDs exert two kinds of functions, including energy production during both nutrient and oxygen deprivation, to prevent lipotoxicity induced by excess fatty acid accumulation.[29,30] Thus, LDs have been reported to be involved in cancer development and anticancer therapies,[31,32] and the intricate regulation of LDs could be targeted for drug development.[32] We thus examined whether inhibition of the cellular viability was caused by decreased TG synthesis and LD formation in matairesinol-treated CRC cells. Matairesinol treatment significantly inhibited LD formation in HCT116 and HT29 cells as indicated by the fluorescence staining with BODIPY 493/503 (Figure S5A). The same as the results *in vitro*, IHC staining revealed that CRC mice treated with matairesinol displayed much fewer positive signals of Tip47, a marker of LD membrane (Figure S5B, C). Fragmented mitochondria formation (Figure S5D) and elevated levels of ROS (Figure S5E, F) were observed in HCT116 and HT29 cells after being treated with matairesinol. N-acetylcysteine (NAC), the ROS scavenger, significantly blunted matairesinol-induced ROS production in both CRC cells. Similarly, matairesinol treatment significantly increased the level of ROS in the colon of CRC mice compared with that in AOM/DSS-induced CRC mice (Figure S5G). Additionally, matairesinol treatment significantly induced apoptosis in both CRC cells (Figure S6A−C) and in CRC mice (Figure S6D). Western blot analysis showed that matairesinol treatment resulted in high levels of cytochrome c release from damaged mitochondria to the cytosol and increased the expressions of cleaved caspase-3 and cleaved caspase-9 proteins (Figure S6E). We further examined whether matairesinol induced mitochondrial injury in a manner involving an altered level of ATP in CRC cells and mice. As expected, matairesinol treatment significantly

https://doi.org/10.1021/acs.nanolett.3c00035
Nano Lett. XXXX, XXX, XXX−XXX

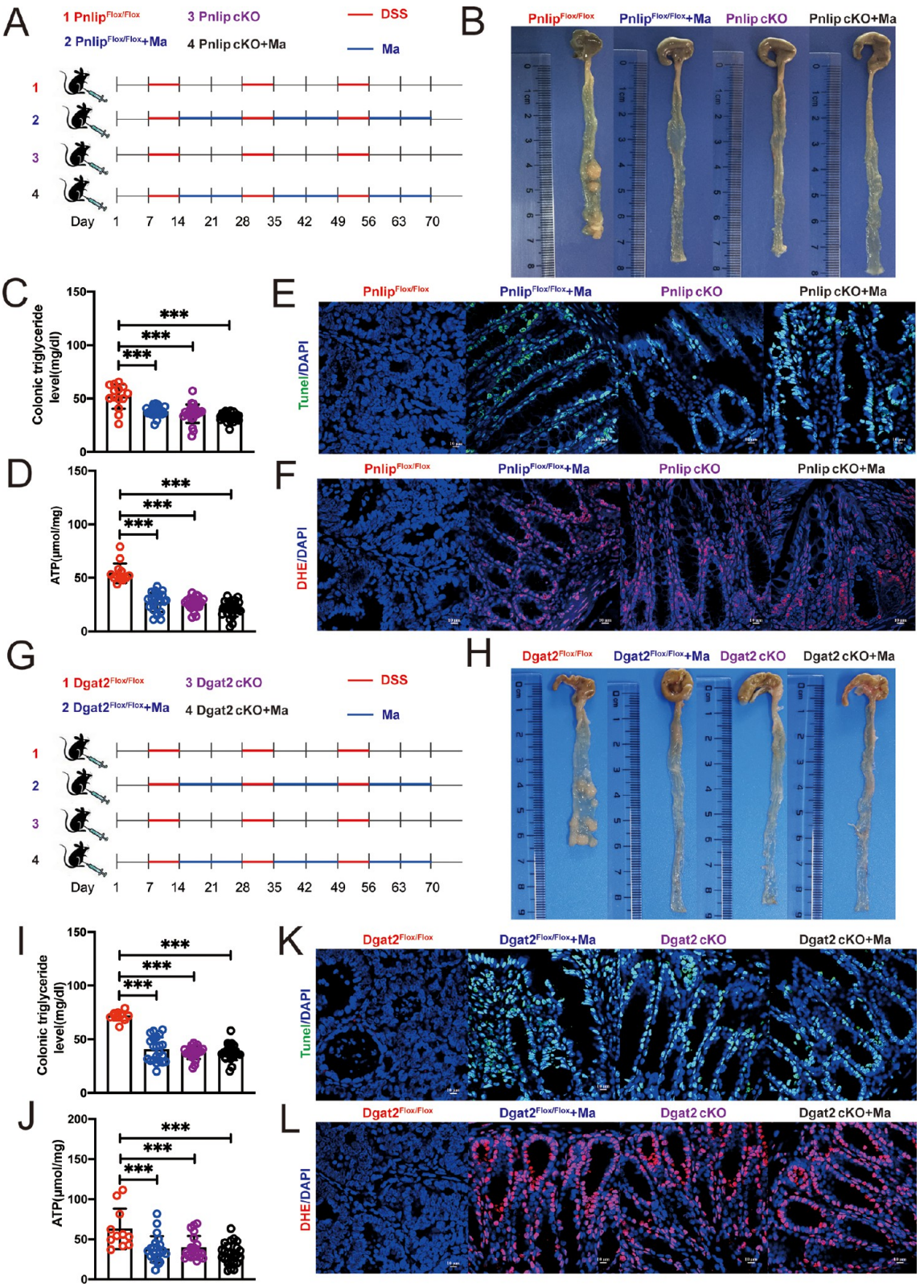

Figure 3. Ablation of *Pnlip* or *Dgat2* inhibits CRC development. (A) Schematic of the generation of colitis-associated CRC model in intestine *Pnlip* knockout mice (n = 30/group). (B) Representative murine colon tissue images of the intestine *Pnlip* knockout mice following AOM-DSS administration. (C). Quantification of colonic TGs in murine colon tissues of the intestine *Pnlip* knockout mice (n = 14 in the $Pnlip^{Flox/Flox}$ group, n = 22 in the $Pnlip^{Flox/Flox}$ and matairesinol-treated group, n = 24 in the *Pnlip* cKO group, n = 25 in the *Pnlip* cKO and matairesinol-treated mice, ***P < 0.001, compared with the $Pnlip^{Flox/Flox}$ group, one-way ANOVA, error bars, S.D.). (D) Quantification of colonic ATPs in murine colon tissues of the intestine *Pnlip* knockout mice (n = 14 in the $Pnlip^{Flox/Flox}$ group, n = 22 in the $Pnlip^{Flox/Flox}$ and matairesinol-treated group, n = 24 in the *Pnlip* cKO group, n = 25 in the *Pnlip* cKO and matairesinol-treated mice, ***P < 0.001, compared with the $Pnlip^{Flox/Flox}$ group, one-way ANOVA, error bars, S.D.). (E). Representative fluorescence images of apoptosis (green) detected with Tunel staining in murine colon tissue of *Pnlip* knockout mice. Nuclei were stained with DAPI (blue). (F) Representative fluorescence images of ROS (red) detected with DHE staining in

https://doi.org/10.1021/acs.nanolett.3c00035
Nano Lett. XXXX, XXX, XXX−XXX

Figure 3. continued

murine colon tissue of *Pnlip* knockout mice. Nuclei were stained with DAPI (blue). (G) Schematic of the generation of colitis-associated CRC model in intestine *Dgat2* knockout mice (n = 30/group). (H) Representative murine colon tissue images of the intestine *Dgat2* knockout mice following AOM-DSS administration. (I). Quantification of colonic TGs in murine colon tissues of the intestine *Dgat2* knockout mice (n = 11 in the $Dgat2^{Flox/Flox}$ group, n = 22 in the $Dgat2^{Flox/Flox}$ and matairesinol-treated group, n = 21 in the *Dgat2* cKO group, n = 24 in the *Dgat2* cKO and matairesinol-treated mice, ***$P < 0.001$, compared with the $Dgat2^{Flox/Flox}$ group, one-way ANOVA, error bars, S.D.). (J) Quantification of colonic ATPs in murine colon tissues of the intestine *Dgat2* knockout mice (n = 11 in the $Dgat2^{Flox/Flox}$ group, n = 22 in the $Dgat2^{Flox/Flox}$ and matairesinol-treated group, n = 21 in the *Dgat2* cKO group, n = 24 in the *Dgat2* cKO and matairesinol-treated mice, ***$P < 0.001$, compared with the group, one-way ANOVA, error bars, S.D.). (K) Representative fluorescence images of apoptosis (green) detected with Tunel staining in murine colon tissue of the intestine *Dgat2* knockout mice. Nuclei were stained with DAPI (blue). (L) Representative fluorescence images of ROS (red) detected with DHE staining in murine colon tissue of the intestine *Dgat2* knockout mice. Nuclei were stained with DAPI (blue).

decreased ATP levels in HCT116 and HT29 cells (Figure S6F) and in AOM/DSS-induced CRC mice (Figure S6G). These results indicated that matairesinol treatment leads to inhibition of LD formation, which increases mitochondrial fragment and damage, ROS production, and apoptosis in the treatment of CRC.

To functionally test the role of *Pnlip* in CRC development, we generated an intestinal conditional *Pnlip* knockout mouse model (*Pnlip* cKO) by using the Flox/Cre system (Figure S7A), and then employed $Pnlip^{Flox/Flox}$ and *Pnlip* cKO mice for further experiments (Figure 3A). *Pnlip* cKO mice treated with AOM and DSS had longer colon lengths (Figure 3B and Figure S7B), decreased tumor numbers (Figure S7C), increased body weights (Figure S7D), and increased survival time (Figure S7E) compared with $Pnlip^{Flox/Flox}$ mice. *Pnlip* cKO mice showed a significantly lower histological score than $Pnlip^{Folx/Flox}$ mice (Figure S7F). Levels of Pnlip and Tip47 protein were downregulated in *Pnlip* cKO mice compared with $Pnlip^{Folx/Flox}$ mice (Figure S7G, H). *Pnlip* knockout significantly decreased the levels of colonic TGs (Figure 3C) and ATP (Figure 3D) and increased apoptosis (Figure 3E) and ROS levels in AOM/DSS-treated mice (Figure 3F). As expected, matairesinol significantly inhibited CRC development in $Pnlip^{Flox/Flox}$ mice and mildly increased the therapeutic efficacy of AOM/DSS-treated *Pnlip* cKO mice (Figure 3A−F and Figure S7A−H), indicating that matairesinol represses CRC tumorigenesis by partly downregulating *Pnlip*.

By using a similar strategy, we generated conditional intestine *Dgat2* knockout mice (Figure S8A) and found that intestine *Dgat2* ablation attenuated CRC development by inducing ROS elevation, apoptosis, and inhibiting ATP production (Figure 3G−L and Figure S8A−H). Taken together, these results corroborate that matairesinol protects against CRC development by down-regulating *Pnlip* and *Dgat2*.

Given the demonstrated role of matairesinol in inhibiting the CRC development *in vivo*, we speculated that matairesinol might enhance chemosensitivity for CRC. We first measured the contents of matairesinol in 521 patients with metastatic CRC, whose intact chemotherapy information was available.[33] The concentration of matairesinol in corresponding plasma samples was 0.1012 ± 0.079 μg/L. IHC analysis showed significantly less positive staining of PNLIP, DGAT2, and TIP47 in tumor tissues of CRC patients with high matairesinol levels compared to CRC patients with low matairesinol (Figure S9A, B). Plasma matairesinol levels were positively correlated with overall survival and progression-free survival in 521 CRC patients (Figure S10A, B). Furthermore, patients with high levels of plasma matairesinol had a significantly greater chance of achieving clinical benefit from FOLFOX treatment, compared to those with low matairesinol levels (Table S2), indicating that matairesinol sensitizes colorectal cancer to the FOLFOX regimen.

It has been shown that matairesinol is a dibenzylbutyrolactone lignan consisting of two aromatic rings (aryl groups) linked with a seven-carbon chain, which is another subclass of natural nonflavonoid polyphenols.[34,35] However, the probable use of the polyphenolic compounds in humans is particularly restricted by several factors, the most common being its insoluble nature, i.e., insolubility, impermeability, fast release, low bioavailability, and ability to be influenced by various environmental factors (heat, temperature, moisture, etc.). Low solubility leads to low bioavailability; therefore, to promote the enhanced therapeutic efficacy of matairesinol in combination with FOLFOX in CRC, matairesinol-encapsulated liposomes (Liposome-Ma) were prepared, and the enhanced antitumor activity was investigated in HCT116 and HT29 CRC human colon tumor-bearing nude mice. Representative transmission electron microscopy (TEM) images confirmed the spherical structure of the blank liposome and Liposome-Ma (Figure 4A). The hydrodynamic size, polydispersity index (PDI), and average surface potential were 66.1 ± 0.4 nm, 0.17 ± 0.02, and −23.4 ± 0.9 mV for blank liposomes and 81.0 ± 4.3 nm, 0.17 ± 0.02, and −33.7 ± 2.4 mV for Liposome-Ma, respectively (Figure 4B−E). The encapsulation efficiency of matairesinol in Liposome-Ma was 85%, and matairesinol was efficiently loaded in liposomes with a drug loading content of 9.8%, as measured by UV−vis spectrophotometry (Figure 4F).

HCT116 (Figure 4G−J) and HT29 (Figure S11A−E) derived CDX mice were treated with the FOLFOX regimen or in combination with matairesinol. FOLFOX treatment significantly decreased the tumor volume in CDX mice, and treatment with the FOLFOX-matairesinol combination strongly reduced the CRC tumor burden compared with FOLFOX treatment alone (Figure 4G, H and Figure S11A, B). Histological examination also revealed that FOLFOX plus matairesinol treatment, but not FOLFOX alone, decreased the positive staining of PNLIP, DGAT2, and TIP47 in xenograft tumors compared with CRC control (Figure 4I, J and Figure S11C, D). Relative to the untreated group, the expression of the proliferative marker, K_i-67, was significantly decreased in tumors from the combination (matairesinol and FOLFOX) or FOLFOX alone groups, especially for combination treatment (Figure 4I, J and Figure S11C, D). Increased apoptosis and ROS levels of tumor cells were found in the combination treatment group (Figure 4K and Figure S11E). In addition, liposome-Ma strongly enhanced synergized with FOLFOX in CRC therapy compared with matairesinol treatment, as evidenced by significantly decreased the tumor volume, positive staining of PNLIP, DGAT2, TIP47, and K_i-67, and

https://doi.org/10.1021/acs.nanolett.3c00035
Nano Lett. XXXX, XXX, XXX−XXX

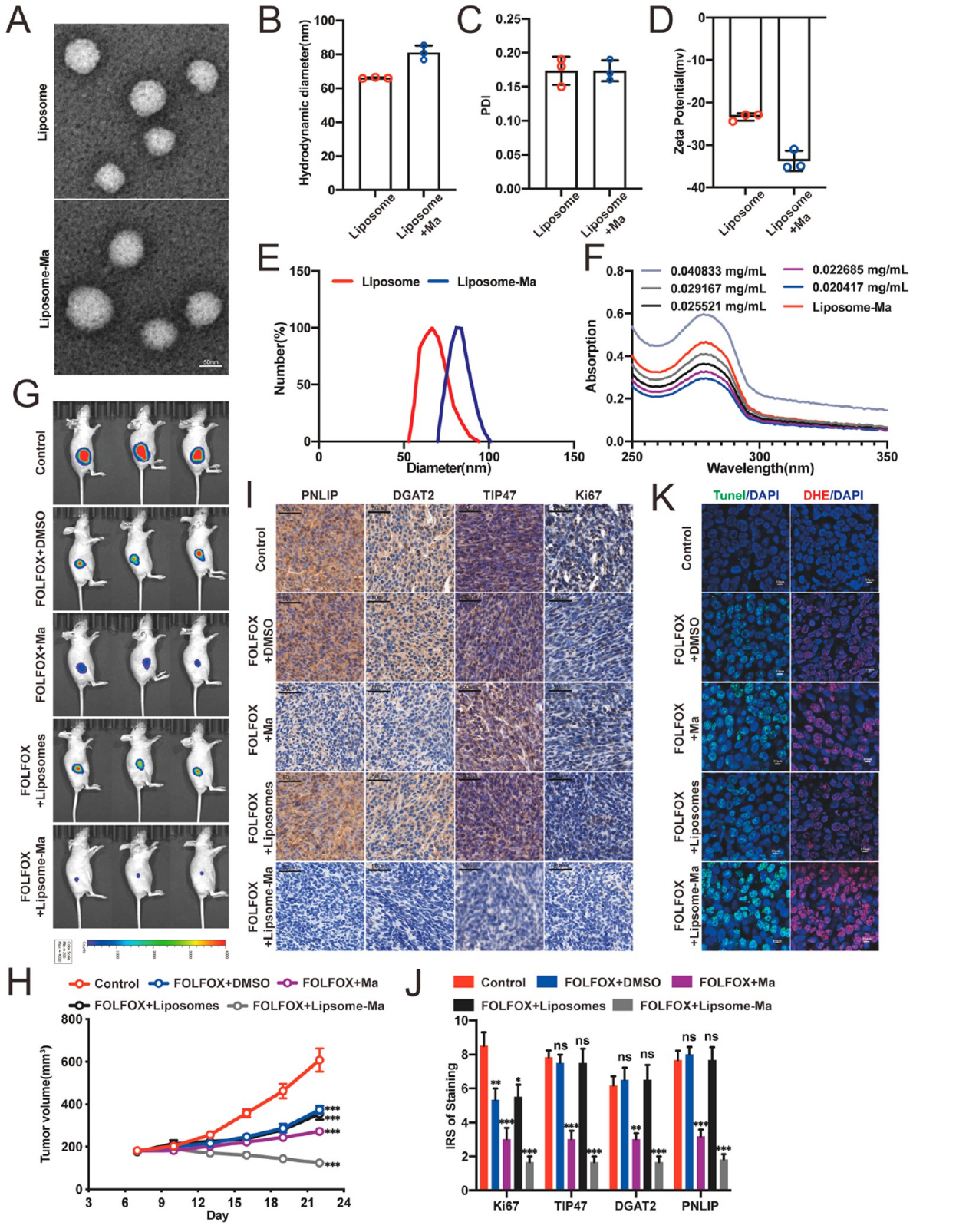

Figure 4. Matairesinol-loaded liposomes sensitize colorectal cancer to the FOLFOX regimen in the HCT116 cell derived CDX mice model. (A) TEM image of blank liposome and matairesinol liposome. (B–D) The (B) average size, (C) polydispersity index (PDI), and (D) surface charges of blank liposome and matairesinol liposome. (E) Size distribution of blank liposome and matairesinol liposome. (F) UV–vis spectrum of different concentrations of matairesinol. (G–J) Effect of FOLFOX and matairesinol on (G, H) flank tumor burden and (I, J) PNLIP, DGAT2, TIP47, and Ki67 staining of HCT116 nude mice (n = 6 in each, ***P < 0.001, *P < 0.05, compared with the control group, one-way ANOVA, error bars, S.D.). (K) Representative fluorescence images of apoptosis (green) and ROS (red) were detected with Tunel and DHE staining in flank tumors of HCT116 nude mice, respectively. Nuclei were stained with DAPI (blue).

https://doi.org/10.1021/acs.nanolett.3c00035
Nano Lett. XXXX, XXX, XXX−XXX

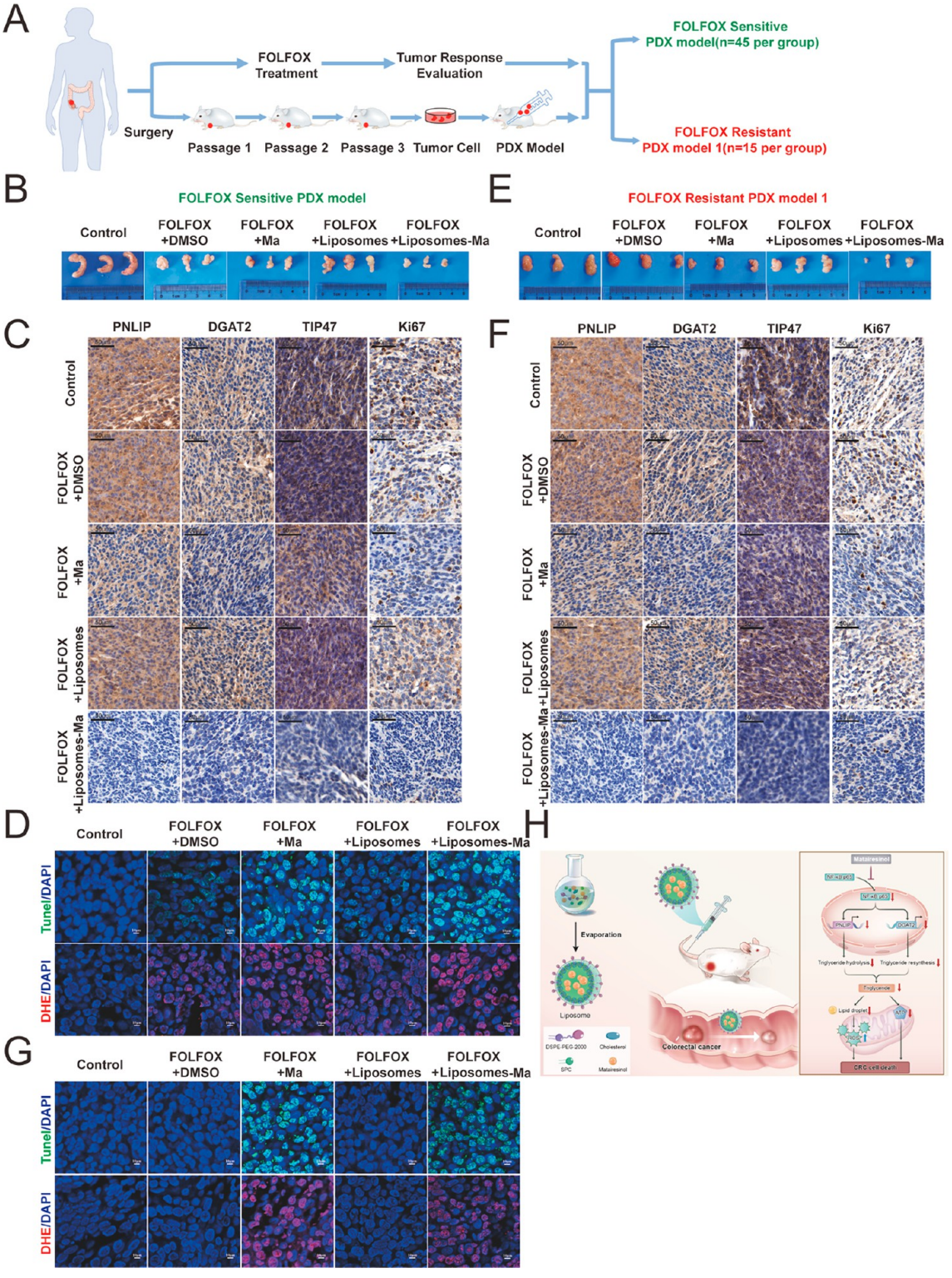

Figure 5. Matairesinol-loaded liposomes sensitize colorectal cancer to the FOLFOX regimen in a PDX mice model. (A) Schematic of the FOLFOX-sensitive PDX model and FOLFOX-resistant PDX model 1. (B, C) Effect of FOLFOX and matairesinol on (B) Oxter tumor burden and (C) PNLIP, DGAT2, TIP47, and Ki67 staining in FOLFOX-sensitive PDX model mice treated with FOLFOX and (or) matairesinol (n = 45 in each). (D) Representative fluorescence images of apoptosis (green) and ROS (red) detected with Tunel and DHE staining in the Oxter tumor of FOLFOX-sensitive PDX model mice, respectively. Nuclei were stained with DAPI (blue). (E, F). Effect of FOLFOX and matairesinol on (E) Oxter tumor burden and (F) PNLIP, DGAT2, TIP47, and Ki67 staining in FOLFOX-resistant PDX model 1 mice treated with FOLFOX and (or) matairesinol (n = 15 in each). (G) Representative fluorescence images of apoptosis (green) and ROS (red) detected with Tunel staining in the Oxter tumor of FOLFOX-resistant PDX model 1 mice, respectively. Nuclei were stained with DAPI (blue). (H). Schematic of CRC development and key modulators affected by matairesinol.

https://doi.org/10.1021/acs.nanolett.3c00035
Nano Lett. XXXX, XXX, XXX−XXX

increased apoptosis and ROS levels in HCT116 and HT29 CRC human colon tumor-bearing nude mice (Figure 4G−J and Figure S11A−E).

Tumor tissues collected from 20 CRC patients were used to establish the PDX model (Table S3). Based on the consequence of FOLFOX treatment, the PDX model mice were assigned into the FOLFOX-sensitive group and the FOLFOX-resistant PDX model 1 group (Figure 5A). For the FOLFOX-sensitive group, the patients were known to have no tumor recurrence after the first time of surgery and FOLFOX chemotherapy. Fresh human CRC tissues obtained from primary surgery of CRC patients were used to establish a FOLFOX-sensitive PDX model (Figure 5A). We found that FOLFOX and matairesinol combination treatment had an inhibitory effect on tumor growth (Figure 5B and Figure S12A). Positive staining of PNLIP, DGAT2, and TIP47 was significantly downregulated in matairesinol and FOLFOX-treated mice, but not FOLFOX alone, as determined by IHC (Figure 5C and Figure S12B). Markedly attenuated expression of K_i-67 (Figure 5C and Figure S12B) and increased apoptosis (Figure 5D) and ROS levels (Figure 5D) were observed in tumors from the combination or FOLFOX alone treatment compared with untreated mice, especially for the combination treatment. For the FOLFOX-resistant group, matairesinol treatment significantly reduced the tumor burden (Figure 5E and Figure S12C). Levels of PNLIP, DGAT2, TIP47, and K_i-67 proteins, apoptosis, and ROS production were consistently decreased in matairesinol-treated, but not FOLFOX alone treated mice (Figure 5F and Figure S12D). In addition, we collected CRC tissues at the second time of surgery in relapse patients and established the FOLFOX-resistant PDX model 2 (Figure S13A). Again, we observed a similar trend in both tumor burden, protein levels of PNLIP, DGAT2, TIP47, and K_i-67, and apoptosis and ROS levels in matairesinol-treated or FOLFOX alone treated mice (Figure S13B−F). Moreover, liposome-Ma treatment significantly reduced the tumor burden in both FOLFOX-sensitive and FOLFOX-resistant PDX model mice, compared with matairesinol treatment (Figure 5A−G and Figure S13A−F). To evaluate the safety of the liposome-mediated matairesinol delivery, we then performed H&E staining in the heart, liver, lung, or kidney of CDX and PDX model mice. As shown in Figure S13, we did not observe any pathological damage in the heart, liver, lung, or kidney in either CDX (Figure S14A) or PDX (Figure S14B) model mice, suggesting the liposomes were safe and biocompatible drug carriers for matairesinol delivery.

In our study, we demonstrated the role of matairesinol in CRC inhibition through attenuation of LD accumulation. However, whether other mechanisms are involved in CRC development needs to be further explored. For example, during gut homeostasis, mitochondrial β-oxidation of fatty acids causes epithelial hypoxia, which maintains anaerobiosis in the lumen of the gut, suggesting matairesinol treatment might disrupt gut anaerobiosis through damaging mitochondrial.[36,37] Further, the anaerobic bacterium, for example, Fusobacterium nucleatum promotes colorectal carcinogenesis through the microbiome-derived metabolites.[38] Thus, matairesinol-loaded liposomes might inhibit CRC by modulating the microbiota metabolism. In addition, LDs modulate the crosstalk between tumor cells and immune cells, such as tumor-associated macrophages (TAMs), myeloid-derived suppressor cells (MDSCs), and dendritic cells (DCs), suggesting the roles of LDs in regulating the tumor microenvironment.[31]

In conclusion, these findings supported the notion that matairesinol was a novel antitumor adjuvant for CRC therapy by rewiring lipid metabolism, and liposomes can be used as potential drug delivery to improve the therapeutic efficacy of matairesinol in CRC treatment through recovering chemosensitivity and enhancing the enhanced antitumor activity of FOXFOL for CRC therapy (Figure 5H).

■ ASSOCIATED CONTENT

Supporting Information

The Supporting Information is available free of charge at https://pubs.acs.org/doi/10.1021/acs.nanolett.3c00035.

Experimental section; quantification of the metabolite in plasma samples of patients with CRC and healthy controls (Figure S1); effects of matairesinol on viability of CRC cells and colon length and body weight of the colitis-associated cancer model mice (Figure S2); effect of matairesinol on PNLIP and DGAT2 expression (Figure S3); matairesinol regulates PNLIP and DGAT2 expression by inhibiting NF-κB p65 activity (Figure S4); matairesinol induces mitochondrial damage, and ROS elevation by inhibiting LD storage in CRC cells (Figure S5); matairesinol induces cell apoptosis and reduces ATP production in CRC cells (Figure S6); effects of *Pnlip* intestine conditional knockout on CRC (Figure S7); effects of Dgat2 intestine conditional knockout on CRC (Figure S8); PNLIP, DGAT2 and TIP47 expression in CRC patients (Figure S9); survival information for patients with CRC and different matairesinol levels (Figure S10); matairesinol-loaded liposomes sensitize colorectal cancer to FOLFOX regimen in HT29 cell derived CDX mice model (Figure S11); matairesinol-loaded liposome reduces PDX tumor burden in FOLFOX-sensitive PDX model and FOLFOX-resistant PDX model 1 mice (Figure S12); matairesinol-loaded liposomes sensitize colorectal cancer to FOLFOX regimen in a FOLFOX-resistant PDX model (Figure S13); systematic toxicity assessment of liposomes (Figure S14); frequency distribution of the selected variables in colorectal cancer cases and controls (Table S1); association between Mat levels and response rates, colorectal cancer patient's survival (Table S2); clinical characteristics of the patients used for developing PDX models (Table S3) (PDF)

■ AUTHOR INFORMATION

Corresponding Authors

Rui Chen − *School of Public Health, Capital Medical University, Beijing 100069, P.R. China; Advanced Innovation Center for Human Brain Protection, Capital Medical University, Beijing 100069, P. R. China; Beijing Laboratory of Allergic Diseases, Capital Medical University, Beijing 100069, P.R. China; Institute for Chemical Carcinogenesis, Guangzhou Medical University, Guangzhou 511436, P.R. China*; orcid.org/0000-0001-9239-0891; Email: ruichen@ccmu.edu.cn

Hanqing Chen − *Guangzhou First People's Hospital, School of Medicine, South China University of Technology, Guangzhou 510180, P.R. China*; Email: chenhq921@163.com

https://doi.org/10.1021/acs.nanolett.3c00035
Nano Lett. XXXX, XXX, XXX−XXX

Authors

Shenshen Wu − *School of Public Health, Capital Medical University, Beijing 100069, P.R. China*

Jiajia Wang − *School of Public Health, Capital Medical University, Beijing 100069, P.R. China*

Zan Fu − *Department of General Surgery, The First Affiliated Hospital of Nanjing Medical University, Nanjing 210029, P.R. China*

Giuseppe Familiari − *Department of Anatomical, Histological, Medical and Legal Locomotive Apparatus, Section of Human Anatomy Via Alfonso Borelli, Sapienza University of Rome, Roma 5000161, Italia;* orcid.org/0000-0002-3456-1434

Michela Relucenti − *Department of Anatomical, Histological, Forensic Medicine and Orthopedic Science, Sapienza University of Rome, Roma 5000161, Italia*

Michael Aschner − *Department of Molecular Pharmacology, Albert Einstein College of Medicine, Bronx, New York 10461, United States*

Xiaobo Li − *School of Public Health, Capital Medical University, Beijing 100069, P.R. China; Key Laboratory of Environmental Medicine Engineering, Ministry of Education, School of Public Health, Southeast University, Nanjing 210009, P.R. China*

Complete contact information is available at: https://pubs.acs.org/10.1021/acs.nanolett.3c00035

Author Contributions

Conceptualization: R.C., H.Q.C., S.S.W.; Methodology: S.S.W., J.J.W., Z.F.; Investigation: S.S.W.; Visualization: S.S.W., J.J.W.; Funding acquisition: R.C., X.B.L., H.Q.C., S.S.W., M.A.; Project administration: R.C., S.S.W.; Supervision: R.C., H.Q.C.; Writing−original draft: X.B.L., S.S.W.; Writing−review and editing: R.C.,. H.Q.C., M.A., M.R., G.F.

Notes

The authors declare no competing financial interest.

■ ACKNOWLEDGMENTS

This work was financially supported by the National Science Fund for Distinguished Young Scholars (82025031), the State Key Program of the National Natural Science Foundation of China (82230109), the National Natural Science Foundation of China (82003499, 32171370, 82241084, 81973084), the Scientific Research Common Program of Beijing Municipal Commission of Education (KM202110025206), the Youth Beijing Scholar Program, and the National Institute of Environmental Health Sciences (NIEHS) (R01 ES10563, R01 ES07331, and R01 ES020852).

■ REFERENCES

(1) Dekker, E.; Tanis, P. J.; Vleugels, J. L. A.; Kasi, P. M.; Wallace, M. B. Colorectal cancer. *Lancet* **2019**, *394*, 1467−1480.

(2) Longley, D. B.; Johnston, P. G. Molecular mechanisms of drug resistance. *Journal of pathology* **2005**, *205*, 275−292.

(3) Bernini, P.; Bertini, I.; Luchinat, C.; Nincheri, P.; Staderini, S.; Turano, P. Standard operating procedures for pre-analytical handling of blood and urine for metabolomic studies and biobanks. *J. Biomol NMR* **2011**, *49*, 231−243.

(4) Brasili, E.; Filho, V. C. Metabolomics of cancer cell cultures to assess the effects of dietary phytochemicals. *Crit Rev. Food Sci. Nutr* **2017**, *57*, 1328−1339.

(5) Zaimenko, I.; Jaeger, C.; Brenner, H.; Chang-Claude, J.; Hoffmeister, M.; Grotzinger, C.; Detjen, K.; Burock, S.; Schmitt, C. A.; Stein, U.; Lisec, J. Non-invasive metastasis prognosis from plasma metabolites in stage II colorectal cancer patients: The DACHS study. *International journal of cancer* **2019**, *145*, 221−231.

(6) Asiago, V. M.; Alvarado, L. Z.; Shanaiah, N.; Gowda, G. A.; Owusu-Sarfo, K.; Ballas, R. A.; Raftery, D. Early detection of recurrent breast cancer using metabolite profiling. *Cancer research* **2010**, *70*, 8309−8318.

(7) Wishart, D. S. Emerging applications of metabolomics in drug discovery and precision medicine. *Nature reviews. Drug discovery* **2016**, *15*, 473−484.

(8) van Asten, J. J.; Vettukattil, R.; Buckle, T.; Rottenberg, S.; van Leeuwen, F.; Bathen, T. F.; Heerschap, A. Increased levels of choline metabolites are an early marker of docetaxel treatment response in BRCA1-mutated mouse mammary tumors: an assessment by ex vivo proton magnetic resonance spectroscopy. *J. Transl Med.* **2015**, *13*, 114.

(9) Wettersten, H. I.; Hakimi, A. A.; Morin, D.; Bianchi, C.; Johnstone, M. E.; Donohoe, D. R.; Trott, J. F.; Aboud, O. A.; Stirdivant, S.; Neri, B.; Wolfert, R.; Stewart, B.; Perego, R.; Hsieh, J. J.; Weiss, R. H. Grade-Dependent Metabolic Reprogramming in Kidney Cancer Revealed by Combined Proteomics and Metabolomics Analysis. *Cancer research* **2015**, *75*, 2541−2552.

(10) Jacob, M.; Lopata, A. L.; Dasouki, M.; Abdel Rahman, A. M. Metabolomics toward personalized medicine. *Mass Spectrom Rev.* **2019**, *38*, 221−238.

(11) Miyagi, Y.; Higashiyama, M.; Gochi, A.; Akaike, M.; Ishikawa, T.; Miura, T.; Saruki, N.; Bando, E.; Kimura, H.; Imamura, F.; Moriyama, M.; Ikeda, I.; Chiba, A.; Oshita, F.; Imaizumi, A.; Yamamoto, H.; Miyano, H.; Horimoto, K.; Tochikubo, O.; Mitsushima, T.; Yamakado, M.; Okamoto, N. Plasma free amino acid profiling of five types of cancer patients and its application for early detection. *PLoS One* **2011**, *6*, No. e24143.

(12) Zhu, J.; Djukovic, D.; Deng, L.; Gu, H.; Himmati, F.; Abu Zaid, M.; Chiorean, E. G.; Raftery, D. Targeted serum metabolite profiling and sequential metabolite ratio analysis for colorectal cancer progression monitoring. *Anal Bioanal Chem.* **2015**, *407*, 7857−7863.

(13) Bertini, I.; Cacciatore, S.; Jensen, B. V.; Schou, J. V.; Johansen, J. S.; Kruhoffer, M.; Luchinat, C.; Nielsen, D. L.; Turano, P. Metabolomic NMR fingerprinting to identify and predict survival of patients with metastatic colorectal cancer. *Cancer research* **2012**, *72*, 356−364.

(14) Leichtle, A. B.; Nuoffer, J. M.; Ceglarek, U.; Kase, J.; Conrad, T.; Witzigmann, H.; Thiery, J.; Fiedler, G. M. Serum amino acid profiles and their alterations in colorectal cancer. *Metabolomics* **2012**, *8*, 643−653.

(15) Rachieriu, C.; Eniu, D. T.; Mois, E.; Graur, F.; Socaciu, C.; Socaciu, M. A.; Hajjar, N. A. Lipidomic Signatures for Colorectal Cancer Diagnosis and Progression Using UPLC-QTOF-ESI(+)MS. *Biomolecules* **2021**, *11*, 417.

(16) Nair, A. B.; Jacob, S. A simple practice guide for dose conversion between animals and human. *J. Basic Clin Pharm.* **2016**, *7*, 27−31.

(17) Shen, S.; Yang, L.; Li, L.; Bai, Y.; Cai, C.; Liu, H. A plasma lipidomics strategy reveals perturbed lipid metabolic pathways and potential lipid biomarkers of human colorectal cancer. *J. Chromatogr B Analyt Technol. Biomed Life Sci.* **2017**, *1068-1069*, 41−48.

(18) Fhaner, C. J.; Liu, S.; Ji, H.; Simpson, R. J.; Reid, G. E. Comprehensive lipidome profiling of isogenic primary and metastatic colon adenocarcinoma cell lines. *Anal. Chem.* **2012**, *84*, 8917−8926.

(19) Yen, C. L.; Stone, S. J.; Koliwad, S.; Harris, C.; Farese, R. V., Jr. Thematic review series: glycerolipids. DGAT enzymes and triacylglycerol biosynthesis. *J. Lipid Res.* **2008**, *49*, 2283−2301.

(20) Chatzigeorgiou, A.; Kandaraki, E.; Papavassiliou, A. G.; Koutsilieris, M. Peripheral targets in obesity treatment: a comprehensive update. *Obes Rev.* **2014**, *15*, 487−503.

(21) Das, S. K.; Hoefler, G. The role of triglyceride lipases in cancer associated cachexia. *Trends Mol. Med.* **2013**, *19*, 292−301.

(22) Singh, S. P.; Hussain, I.; Konwar, B. K.; Deka, R. C.; Singh, C. B. Design of Potential IKK-beta Inhibitors using Molecular Docking

and Molecular Dynamics Techniques for their Anti-cancer Potential. *Curr. Comput. Aided Drug Des* **2021**, *17*, 83−94.
(23) Wu, Q.; Wang, Y.; Li, Q. Matairesinol exerts anti-inflammatory and antioxidant effects in sepsis-mediated brain injury by repressing the MAPK and NF-kappaB pathways through up-regulating AMPK. *Aging (Albany NY)* **2021**, *13*, 23780−23795.
(24) Grabe, N. AliBaba2: context specific identification of transcription factor binding sites. *In Silico Biol.* **2002**, *2*, S1−S15.
(25) Cotte, A. K.; Aires, V.; Fredon, M.; Limagne, E.; Derangere, V.; Thibaudin, M.; Humblin, E.; Scagliarini, A.; de Barros, J. P.; Hillon, P.; et al. Lysophosphatidylcholine acyltransferase 2-mediated lipid droplet production supports colorectal cancer chemoresistance. *Nat. Commun.* **2018**, *9*, 322.
(26) Walther, T. C.; Chung, J.; Farese, R. V., Jr. Lipid Droplet Biogenesis. *Annual review of cell and developmental biology* **2017**, *33*, 491−510.
(27) Petan, T.; Jarc, E.; Jusovic, M. Lipid Droplets in Cancer: Guardians of Fat in a Stressful World. *Molecules* **2018**, *23*, 1941.
(28) Wilfling, F.; Haas, J. T.; Walther, T. C.; Farese, R. V., Jr. Lipid droplet biogenesis. *Curr. Opin Cell Biol.* **2014**, *29*, 39−45.
(29) Visweswaran, M.; Arfuso, F.; Warrier, S.; Dharmarajan, A. Aberrant lipid metabolism as an emerging therapeutic strategy to target cancer stem cells. *Stem Cells* **2020**, *38*, 6−14.
(30) Cheng, X.; Geng, F.; Pan, M.; Wu, X.; Zhong, Y.; Wang, C.; Tian, Z.; Cheng, C.; Zhang, R.; Puduvalli, V.; et al. Targeting DGAT1 Ameliorates Glioblastoma by Increasing Fat Catabolism and Oxidative Stress. *Cell metabolism* **2020**, *32*, 229−242.e8.
(31) Cruz, A. L. S.; Barreto, E. A.; Fazolini, N. P. B.; Viola, J. P. B.; Bozza, P. T. Lipid droplets: platforms with multiple functions in cancer hallmarks. *Cell Death Dis* **2020**, *11*, 105.
(32) Bacci, M.; Lorito, N.; Smiriglia, A.; Morandi, A. Fat and Furious: Lipid Metabolism in Antitumoral Therapy Response and Resistance. *Trends Cancer* **2021**, *7*, 198−213.
(33) Wu, S.; Yang, X.; Tang, W.; Familiari, G.; Relucenti, M.; Aschner, M.; Li, X.; Chen, R. Chemotherapeutic Risk lncRNA-PVT1 SNP Sensitizes Metastatic Colorectal Cancer to FOLFOX Regimen. *Front Oncol* **2022**, *12*, 808889.
(34) Lee, W.; Song, G.; Bae, H. Matairesinol Induces Mitochondrial Dysfunction and Exerts Synergistic Anticancer Effects with 5-Fluorouracil in Pancreatic Cancer Cells. *Mar Drugs* **2022**, *20*, 473.
(35) Khan, N.; Khan, M. I.; Tabrez, S.; Khan, M. F.; Khan, M. I. In *Polyphenols-Based Nanotherapeutics for Cancer Management*; Tabrez, S., Imran Khan, M., Eds.; Springer, 2021; pp 357−365.
(36) Litvak, Y.; Byndloss, M. X.; Tsolis, R. M.; Baumler, A. J. Dysbiotic Proteobacteria expansion: a microbial signature of epithelial dysfunction. *Curr. Opin Microbiol* **2017**, *39*, 1−6.
(37) Litvak, Y.; Byndloss, M. X.; Baumler, A. J. Colonocyte metabolism shapes the gut microbiota. *Science* **2018**, *362*, No. eaat9076.
(38) Ternes, D.; Tsenkova, M.; Pozdeev, V. I.; Meyers, M.; Koncina, E.; Atatri, S.; Schmitz, M.; Karta, J.; Schmoetten, M.; Heinken, A.; Rodriguez, F.; Delbrouck, C.; Gaigneaux, A.; Ginolhac, A.; Nguyen, T. T. D.; Grandmougin, L.; Frachet-Bour, A.; Martin-Gallausiaux, C.; Pacheco, M.; Neuberger-Castillo, L.; Miranda, P.; Zuegel, N.; Ferrand, J. Y.; Gantenbein, M.; Sauter, T.; Slade, D. J.; Thiele, I.; Meiser, J.; Haan, S.; Wilmes, P.; Letellier, E. The gut microbial metabolite formate exacerbates colorectal cancer progression. *Nat. Metab* **2022**, *4*, 458−475.

https://doi.org/10.1021/acs.nanolett.3c00035
Nano Lett. XXXX, XXX, XXX−XXX